Stratospheric aerosol formed by intense volcanism – sea interaction during the 2022 Hunga Ha'apai eruption

Bengt G. Martinsson, Johan Friberg, Moa K. Sporre

Department of Physics, Lund University, Lund, Sweden

Correspondence to: Bengt G. Martinsson (bengt.martinsson@fysik.lu.se)

Abstract. The Hunga Tonga eruption the 15 January 2022 (HT-22) induced vigorous volcano – sea interaction. Here we study the stratospheric aerosol and water vapor resulting from the eruption using satellite-based instruments: the CALIOP lidar and the Microwave Limb Sounder (MLS). We investigate the stratospheric relative humidity following the record-breaking water vapor injections from the HT-22 eruption, and the particle size of the aerosol. The HT-22 eruption injected its effluents into the deep Brewer-Dobson (BD) branch causing several years of stratospheric perturbation. The long duration, and aerosol concentration among the highest, makes the HT-22 eruption the strongest stratospheric aerosol event since the 1991 Mt. Pinatubo eruption despite a modest SO_2 injection explaining only ~30% of the AOD from the HT-22 eruption according to our estimates. The stratospheric AOD level was established after 2 weeks, or possibly even earlier, which is a short time compared with the usual 2 – 3 months required to reach the maximum AOD following volcanic eruptions. We discuss the sources of the aerosol from the HT-22 eruption in relation to the low emission of SO_2, its e-folding time and volcanological observations of strong interactions with the sea containing not only water but also high concentrations of dissolved substances.

1 Introduction

The stratospheric background conditions are frequently offset by injections of copious amounts of aerosol and gases from explosive volcanic eruptions (Kremser et al., 2016) and intense wildfires forming pyrocumulonimbus clouds (Fromm et al., 2010). These events cause variable stratospheric impact with durations of months to several years (Friberg et al., 2018), which are important to account for in climate models (Schmidt et al., 2018).

The Hunga Tonga – Hunga Ha'apai volcano erupted on 15 January 2022, with a volumetric flow rate an order of magnitude higher than that of the1991 Mt Pinatubo eruption, and formed an umbrella cloud at 31 km and a second cloud at 17 km altitude (Gupta et al., 2022). Further, a record-breaking overshooting plume reached above 50 km (Carr et al., 2022, Proud et al., 2022, Taha et al., 2022). The volcanic explosivity index (VEI) was estimated to be 6, based on seismological observations (Poli and Shapiro, 2022). Despite the high VEI, ash could not be detected in the ice-rich stratospheric clouds from the HT-22 eruption (Gupta et al., 2022), and the UV aerosol index (UVAI) indicates low ash content (Carn et al., 2022). This is further supported by CALIOP (Cloud-Aerosol LIdar with Orthogonal Polarization) measurements finding very low depolarization ratios indicating dominance of spherical particles uncharacteristic of ash (Legras et al., 2022). Additionally, the volcanic layers in the stratosphere contained very low SO_2 amounts for such a strong eruption (Carn et al., 2022).

Widespread damage to the seafloor with runouts exceeding 100 km was caused by volcaniclastic density currents, suggesting a collapsing eruption column entering the sea (Seabrook et al., 2023; Clare et al., 2023). Such a sequence of events where hot volcaniclastic density currents form induces strong interaction with sea water over vast areas, that can supply hot water vapor forming a plume that is buoyant at the base and accelerates as it rises (Mastin et al., 2024). A relatively small eruption can in this way form umbrella clouds the size and altitude of the HT-22 eruption, whereas entrainment of vapor from cold water does not (Mastin et al., 2024). Other possible mechanisms include formation of an explosive steam from superheated water in contact with the erupting magma (Millán et al., 2022).

The stratospheric background aerosol contains mainly sulfurous and carbonaceous components with some extraterrestrial and tropospheric components (Murphy et al., 2007, Kremser et al., 2016, Martinsson et al., 2019). Volcanic aerosol in the stratosphere normally contains large amounts of sulfuric acid formed from sulfur dioxide (SO_2), water, carbonaceous material and ash (Martinsson et al., 2009; Andersson et al., 2013; Friberg et al., 2014). Wildfires produce an aerosol initially dominated by organic and black carbon (Garofalo et al., 2019), where the former component is rapidly removed by photolysis (half-life 10 days) in the stratosphere (Martinsson et al., 2022; Friberg et al., 2023).

The volcanic and wildfire events also affect particle size distribution. During a long period with conditions close to the background, spanning 1998 to 2004, the particle volume mode was $0.2 - 0.3$ μm in diameter, whereas approximately 1 μm in $1992 - 1993$ after the Mt. Pinatubo eruption (Bauman et al., 2003; Wilson et al., 2008). Measurements the second week after the 2017 Canadian wildfire showed particle diameter of $0.6 - 0.7$ μm (Haarig et al., 2018; Hu et al., 2019).

In this work we investigate the stratospheric aerosol resulting from the HT-22 eruption in relation to the volcanological sequence of events during the eruption. We also investigate the interaction of the aerosol with the large amounts of water vapor injected into the stratosphere. The global stratospheric aerosol optical depth (AOD) is studied 1.5 years after the eruption, until the decommission of the NASA satellite CALIPSO (Cloud-Aerosol Lidar and Infrared Pathfinder Satellite Observation) and its lidar sensor CALIOP. Our incrementally developed evaluation software (Andersson et al., 2015; Friberg et al., 2018; Martinsson et al., 2022) based on methodology presented in Vernier et al., (2011) was applied on CALIOP level 1B data. In contrast to limb-oriented methodology, the nadir-oriented CALIOP provides viable results in dense aerosol layers from strong volcanic eruptions and wildfires after correction for attenuation (Martinsson et al., 2022). We also use the satellite Aura sensor MLS for measurements of water vapor and temperature. We find that the SO_2 emissions from the HT-22 eruption cannot alone explain the high AOD level, nor can ash particles. We also find that the aerosol went deep into the stratosphere and that the one-year AOD perturbation due to the HT-22 eruption is the largest since that of Mt. Pinatubo in 1991.

2 Methods

Two satellite-based instruments were used to investigate the stratosphere following the HT-22 eruption. Aerosol measurements were based on the CALIOP lidar aboard CALIPSO, whereas water vapor concentrations and atmospheric temperature were obtained from MLS aboard Aura.

2.1 CALIOP measurements

CALIPSO orbits the globe 14 – 15 times per day between 82° S and 82° N. The vertical resolutions of CALIOP are 30, 60, 180 and 300 m in the altitude ranges <8.2, 8.2 – 20.2, 20.2 – 30.1 and 30.1 – 40 km, respectively (Winker et al., 2007, 2010). The average global stratospheric AOD from the tropopause (obtained from the MERRA-2 reanalysis (Modern-Era Retrospective analysis for Research and Applications)) to 35 km altitude in the stratosphere was computed from version 4-51 of CALIOP level 1B at the wavelength 532 nm using night-time measurements. The stratospheric AOD was computed in three layers: the lowermost stratosphere (LMS, tropopause to 380 K isentrope), the shallow BD branch (380 – 470 K isentropes) and deep BD branch (470 K isentrope – 35 km altitude), where potential temperatures were obtained from MERRA-2 pressures and temperatures. The effective lidar ratio was estimated based on single, intense volcanic layers day 1 – 28 after the eruption. From initial high values (70 sr) the lidar ratio declined to 47.5 ± 10.2 sr. This is close to the commonly used CALIOP effective lidar ratio of 50 sr, which we therefore applied in this study. The attenuated backscatter CALIOP data were corrected by methods described in Martinsson et al. (2022). Based on measured parallel and perpendicularly polarized scattering, the volume depolarization was obtained and converted to particle depolarization ratios with methods described in Martinsson et al. (2022). Data were missing for a week from a few days after the eruption, and a long gap appeared from 21 October to 7 December 2022. Several minor gaps appeared during the first half-year of 2023 the last data produced by CALIOP.

2.2 MLS measurements

Water vapor concentrations were obtained in the 100 – 1 hPa range in 12 levels per decade from the MLS, version 5.0-1.0a, level 2 (Waters et al., 2006). The vertical resolution is 1.3 – 3.6 km (Lambert et al., 2020; Livesey et al., 2020). Data were screened based on error parameters supplied with the data, rendering a large fraction of the volcanic data invalid the first two weeks after the eruption. From the beginning of February 2022, when our evaluation starts, erroneous data became scarce.

Stratospheric temperatures in the pressure range 100 – 1 hPa were obtained from the MLS, which were used primarily to compute relative humidity and potential temperature. The latter allows analysis of transport in relation to isentropic surfaces. The potential temperatures were also used as a common ground in comparisons between MLS and CALIOP, where the native vertical scale of the former is atmospheric pressure and for the latter geometric altitude.

3 Results

This work focuses on the stratospheric aerosol resulting from the HT-22 eruption. The altitude and latitude distributions will be presented here together with the evolution of the stratospheric aerosol extinction coefficients and AOD. However, we start by presenting stratospheric water vapor data from the HT-22 eruption

106   to highlight the contrasting evolution of the two volcanic components. Water vapor data are also used for

107   computations on relative humidity and vertical air motions presented in the Discussion section.

108
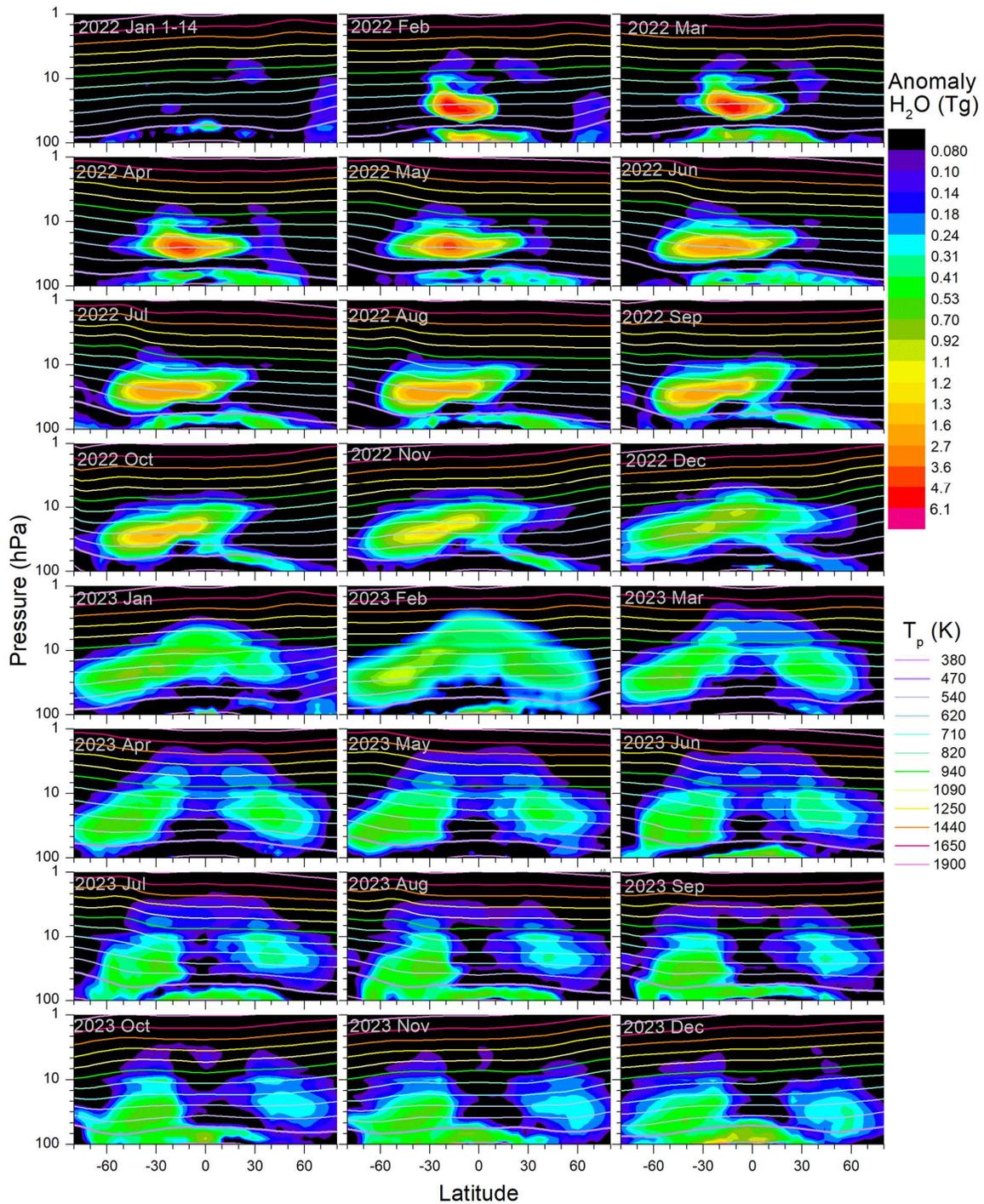
Figure 1. Monthly averaged H_2O mass anomaly (Tg) against latitude and altitude with pixel size (2.3 ± 0.14) x 10^{16} m^3 times $\cos(\Theta)$, where Θ is the latitude. Note that "2022 Jan 1 – 14" covers only the pre-eruption period 1 – 14 January. Overlain isentropes in the range 380 – 1900 K are shown, where T_p is the potential temperature.

112 Note that the 380 K isentrope reaches below 100 hPa only in the tropics and that the 1900 K isentrope partly is

113 found at pressures below 1 hPa. Vertical scale minor ticks: 1.5, 2.2, 3.2, 4.6, 6.8 and ten times these values.

114
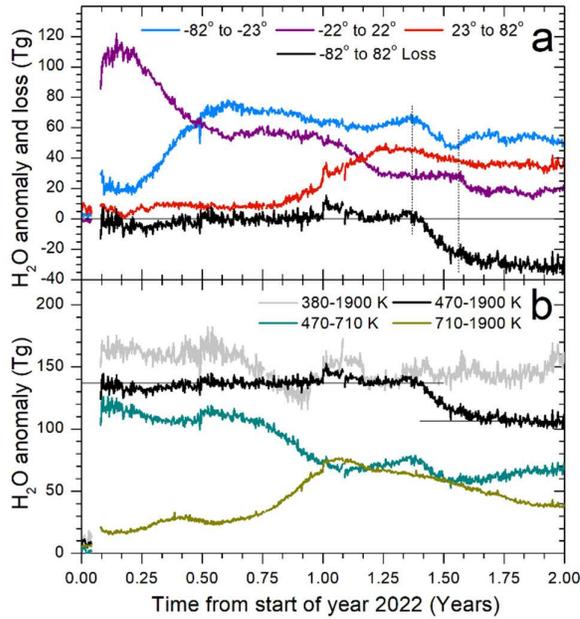
Figure 2. Evolution of water vapor (H_2O) anomaly following the January 15, 2022, Hunga Tonga eruption. **a)**
H_2O anomaly in three latitude intervals and loss of H_2O in a 4th latitude interval, all in the $470 < T_p < 1900$ K
range (the deep BD branch). Vertical lines mark the main region of H_2O loss of the deep BD branch. **b)** H_2O
anomaly in the latitude interval -82 to 82° in various potential temperature intervals (T_p). Horizontal lines show
the average H_2O anomaly from end of January 2022 to mid-May 2023 (136.9±0.2 (standard error) Tg) and from
the beginning of October to the end of December 2023 (106.1±0.3 Tg).

3.1 Water vapor

It has widely been reported about the record-breaking amounts of water vapor reaching the stratosphere
following the HT-22 eruption (Millán et al., 2022; Schoeberl et al., 2022; Xu et al., 2022; Zhu et al., 2022;
Nedoluha et al., 2024). Here we present the distribution related to isentropic surfaces in contrast to previous
authors, in particular the fate of water that reaches the deep branch of the BD circulation, i.e., above the
potential temperature (T_p) 470 K (Fueglistaler et al., 2009). Fig. 1 shows monthly mean water vapor mass
anomalies for years 2022 and 2023, where the masses of year 2021 were subtracted, the exception being January
2022 where only the days prior to the eruption are shown (January 1 – 14). The first two weeks after the
eruption the MLS water vapor data from volcanic effluents frequently were erratic, probably due to high
concentrations, and are not shown.

In February 2022 two layers appear, one minor in the shallow BD branch and the main layer in the deep BD
branch, consistent with the reported eruption chronology (Gupta et al., 2022). The lower water vapor layer is
spread rapidly latitudinally before it is transported below the lower atmospheric pressure limit used here (100
hPa).

The first months after the eruption the water of the upper layer remains in the tropics, before a fraction clearly visible in May 2022 is transported to the Southern extratropics (Figs. 1 and 2a). Towards the end of 2022 transport to the Northern extratropics starts, and in February 2023 the water from the HT-22 eruption covers most of the globe. Later that year most of the water is found in the extratropics, whereas the water-rich air in the tropics is replaced in the BD circulation by younger tropospheric air that is unaffected by the HT-22 eruption (Figs. 1 and 2a). At the same time the water in the Southern extratropics of the deep BD branch approaches and clearly ~~passes~~ descends below the 470 K isentrope in May 2023 (Fig. 1 and 2a), consistent with the extratropical downward motion of air.

The total amount of water vapor from the HT-22 eruption in the stratosphere at $T_p > 380$ K in the tropics and 100 hPa atmospheric pressure elsewhere, is 160 Tg. The mass in the deep BD branch, which is a part of the previously mentioned layer, is 13~~7~~8 Tg. After ¾ of a year these categories reach the same level (Fig. 2b), implying that the lower water layer (injected below the deep BD branch) is transported down below the lower limit in altitude (atmospheric pressure 100 hPa) of the data used here. The water vapor displays considerable vertical transport in the deep BD branch. Dividing that branch into two T_p intervals (Fig. 2b) reveals a clear rise in the amount of water in the upper interval in the last quarter of the year 2022. A small fraction of the water vapor reached high altitudes in the tropics during the year 2023 (Fig. 1), and some even reached altitudes above 1 hPa atmospheric pressure (~48 km), i.e. the region of the stratopause, which can be seen in ~~(~~supplementary Fig. S1~~)~~ but not in Fig. 1 because the much smaller integration volume increases the noise level.

The water anomaly remained constant in the deep BD branch with only minor fluctuations from February 2022 to May 2023 (Fig. 2b), whereafter the anomaly is reduced by 23% due to transport to the shallow BD branch, a level that remains until the end of 2023.

3.2 Aerosol

The evolution of the stratospheric AOD following the HT-22 eruption has been reported by several authors using limb-viewing measurements (Bourassa et al., 2023; Sellitto et al., 2022; Taha et al., 2022) that suffer from event termination ("saturation") during the first months after strong volcanic or wildfire events (Fromm et al., 2014; Chen et al., 2018; DeLand et al., 2019; Martinsson et al., 2022), and problems to measure the lower parts of the stratosphere (Taha, 2020). Here we present results based on a nadir-viewing lidar technique (CALIOP) that is better suited for measurements in dense aerosol layers because they do not suffer from saturation effects, and attenuation of the lidar signal can be corrected for (Martinsson et al., 2022).

Just as for water vapor, we present monthly mean values of the aerosol distribution with overlaid isentropic surfaces (Fig. 3). January 2022 aerosol data show conditions prior to the eruption. Initially (February – June 2022) almost all the HT-22 aerosol is found in the deep BD branch ($T_p > 470$ K). We identify downward motion of the aerosol centroid in the tropics, the most intense part shifting from isentrope 581 to 523 K from March to September 2022, despite the upward motion of air in the tropics as part of the BD circulation. This is caused by gravitational settling, and the aerosol that reaches the Southern extratropics loses altitude even faster, aided by downward air motion in the extratropics, leading to an increasing fraction of the aerosol in the shallow BD

171 branch from July 2022. The aerosol continues downwards, reaching the LMS (below 380 K) in December 2022

172 on its way out of the stratosphere.

173
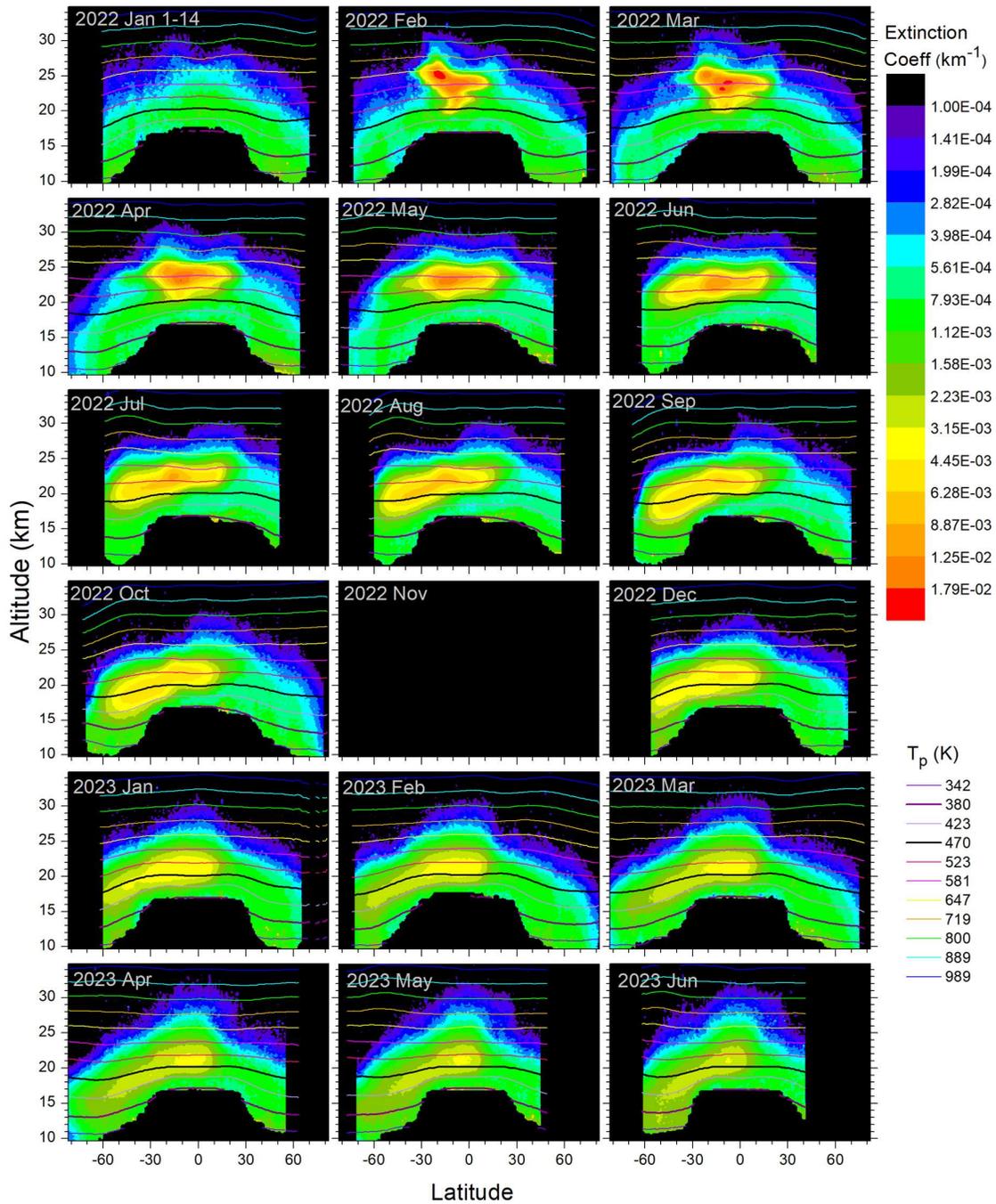
Figure 3. Monthly average extinction coefficients dependent on latitude and altitude with overlaid potential

temperature levels. Note that "2022 Jan 1 – 14" covers only the pre-eruption period 1 – 14 January.

176 Substantial amounts of aerosol entered the stratosphere because of the HT-22 eruption. The global average AOD

177 reached 0.016 (Fig. 4a), which is among the highest stratospheric aerosol loads since the 1991 Mt. Pinatubo

178 eruption. Already by the end of January, half a month after the eruption, the AOD level that remained for almost

179 a year was reached. After that we see a decline where approximately half of the aerosol from the HT-22 eruption

180 is removed during the first half-year of 2023. Almost the entire aerosol amount from HT-22 was found in the

181
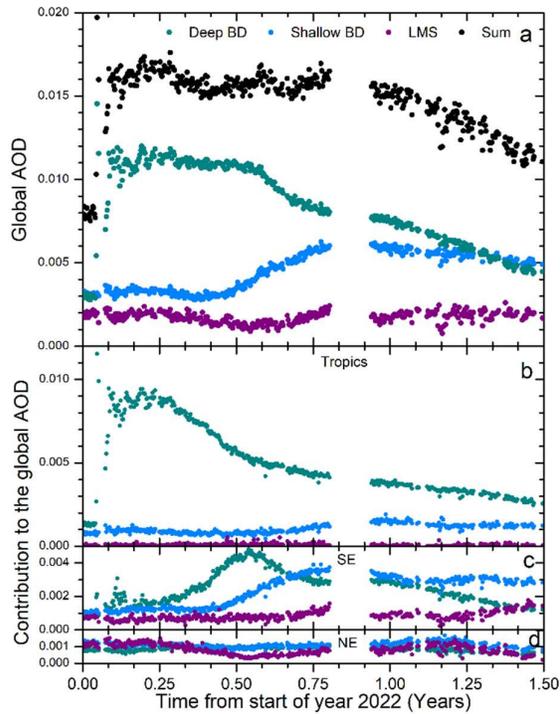
Figure 4. a) Global average AOD of the stratosphere from the tropopause to 35 km altitude and -82 to 82° in

latitude (Sum) with the sub layers: the tropopause to 380 K potential temperature (T_p) (LMS), 380 – 470 K T_p

(shallow Brewer-Dobson (BD) branch) and T_p 470 K to 35 km altitude (deep BD). Latitude distributions of

AOD **b)** tropics (-22 to 22°), **c)** Southern extratropics (SE) (-82 to -23°) and **d)** Northern extratropics (NE) (23

to 82°). The AODs are related to the global scale, i.e. the sum of SE, tropics and NE graphs is the global AOD.

187 deep BD branch the first months after the eruption (Fig. 4a), in the tropics (Fig. 4b). We see transport to the

188 Southern extratropics starting in April 2022 in the deep BD followed by downward motion to the shallow BD

189 branch starting in June 2022 (Fig. 4c). Only a small fraction of the aerosol reached the Northern extratropics

190 (Fig. 4d), in contrast to the transport of water vapor (Fig. 2a) that took place at a higher altitude (Fig.1).

4 Discussion

192 SO_2 emissions from HT-22 eruptions took place over a period from 19 December 2021 to 15 January 2022

193 (Carn 2022). Most of these eruptions reached 15 – 18 km in altitude, whereas the main eruption's umbrella

194 cloud on 15 January 2022 reached 31 km with an overshooting plume reaching 55 – 58 km (Gupta et al., 2022).

195 Based on several methods the total SO_2 emissions during this period is estimated to 0.6 – 0.7 Tg, and that of the

196 main umbrella cloud, reaching deep into the stratosphere, contained 0.4 – 0.5 Tg SO_2 (Carn et al., 2022).

197 Altitude-resolved SO_2 measurements from MLS find a similar SO_2 amount deep into the stratosphere (Millán

198 2022). Compared with the SO_2 emissions, the stratospheric AOD generated by the HT-22 eruption is

199   unexpectedly high. Here we will discuss reasons for this seeming discrepancy, and we start by examining water

200   uptake as an explanation.

201   The temperature is rising with altitude in the stratosphere, making the air very dry after passing the tropical cold

202   point tropopause. The amount of water vapor injected by the HT-22 eruption is unprecedented in the modern

203   satellite era (Zhu et al., 2022). It has been suggested that hygroscopic growth could be an important process that

204   affects the aerosol particle size and light scattering (Legras et al., 2022; Sellitto et al., 2022). Here we investigate

205   the relative humidity by examining the five highest daily water vapor concentrations measured by the MLS

206   during February 2022 (140 MLS profiles), when the volcanic effluents were concentrated to a relatively small

207   volume. Based on MLS water vapor and temperature measurements the relative humidity was computed, where

208   the saturation water vapor pressures were obtained from Murphy and Koop (2005). Fig. 5a shows the average

209   relative humidity of the profiles (140) from February 2022. At the lowest altitudes, close to 100 hPa, the relative

210   humidity reaches 35% because of the low temperature (Fig. 5a, upper scale), and, to a smaller degree, the lower

211   volcanic layer (Fig. 1, February 2022). At higher altitude, the relative humidity rapidly declines as the

212   temperature increases, becoming close to zero at altitudes above 10 hPa. However, a peak appears at 30 hPa

213   caused by the main volcanic layer (above 470 K potential temperature) containing most of the stratospheric

214   water vapor from the HT-22 eruption (Fig. 2b). In the following discussion we concentrate on that layer. The

215   average positions of the 470 K isentrope and the peak water vapor concentration are shown in Fig. 5a, where the

216   shift of the maximum relative humidity from the peak water vapor concentration is caused by the temperature

217   gradient. The relative humidity at the peak water vapor concentration as well as the maximum relative humidity

218   of all the 140 measurements are shown in Fig. 5b (note the shift of $\pm$ 100 K in potential temperature to separate

219   the two categories). The measurements of each of the two categories appear in groups depending on the altitude

220   (or pressure level) of the water vapor layer. The maximum relative humidity above the 470 K isentrope is 13%,

221   and that of the peak water vapor is 11%, whereas the averages are 5.1 and 4.2%. Such low relative humidities

222   causes no or modest hygroscopic growth (Winkler, 1973) that affects particle size or light scattering only to a

223   small degree.

224   Several authors regard the aerosol from the HT-22 eruption as a sulfate aerosol (Khaykin et al., 2022; Legras et

225   al., 2022; Sellitto et al., 2022; Taha et al., 2022; Zhu et al., 2022; Bernath et al., 2023; Duchamp et al., 2023;

226   Kahn et al., 2024; Sellitto et al., 2024), although with questions on the relatively small amount of SO_2 emitted in

227   relation to the AOD level (Carn et al., 2022). Here we will investigate this relation in more detail by forming the

228   ratio of the maximum global stratospheric AOD rise above the pre-eruption AOD to the amount of SO_2 emitted

229   by eight recent volcanic eruptions (Table 1 and Fig. 5c). This ratio is approximately 0.005 Tg^{-1} for most of the

230   eruptions, whereas the Calbuco (Ca-15) and HT-22 deviate by having higher AOD per SO_2 mass emitted. Most

231   of these volcanic eruptions showed depolarization ratio less than 0.05 (Hoffmann et al., 2010; O'Neill et al.,

232   2012; Zhuang & Yi 2016; Voudouri et al., 2023) typical of aerosol dominated by spherical sulfuric acid

233   particles. Volcanic ash settles rapidly by gravitation, but a fraction can remain for months in the stratosphere

234   (Andersson et al., 2013). Vernier et al. (2016) found that this can affect stratospheric AOD, detecting elevated

235   depolarization ratio (0.05) a month after the Kelut eruption (Ke-14). The depolarization ratio of the aerosol from

236   the Ca-15 eruption was much higher (0.18) a month after the eruption (Klekociuk et al., 2020) thus indicating a

237   strong influence from ash on the AOD that likely explains the strong deviation in AOD-to-SO_2 ratio from the

238 other eruptions. Ca-15 was therefore not included in the average AOD-to-SO₂ ratio calculated here. The HT-22

239 eruption has the highest AOD-to-SO₂ ratio but low depolarization ratio (supplementary Fig. S2), thus high ash

240 concentration is not a valid explanation (Gupta et al., 2022; Carn et al., 2022; Legras et al., 2022).

241
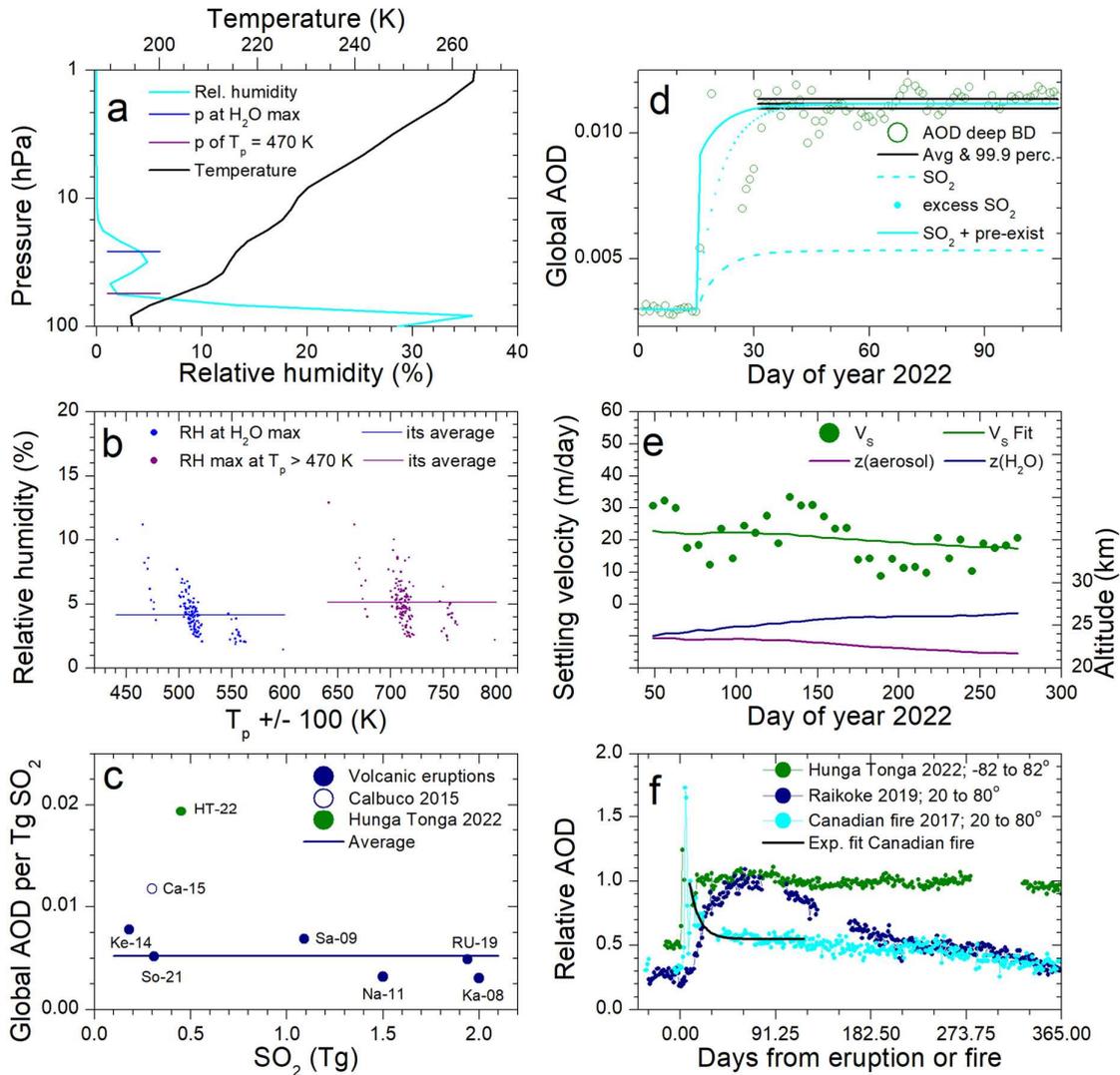
Figure 5. Stratospheric characteristics after the HT-22 eruption. **a)** Average relative humidity (RH) and temperature of the five daily H_2O profiles with the highest concentration during February 2022. **b)** RH at the maximum H_2O concentration and maximum RH at potential temperatures > 470 K of all the profiles mentioned in (a) with average RH of 4.2 and 5.1%, respectively. The potential temperature (T_p) was shifted ± 100 K to separate the two groups of data. **c)** Global AOD per Tg SO_2 emitted by recent volcanic eruptions related to SO_2, the average being 0.0052 global AOD per Tg SO_2 (see Table 1). **d)** AOD in the upper BD branch with 99.9 percentile of the average marked and reported SO_2 of 0.45 Tg (Carn et al., 2022) converted to AOD according to (c) (broken line), and the dotted line tests the evolution using an excess of 1.1 Tg SO_2 to reach the measured AOD. The full cyan line displays the SO_2 AOD (broken line) added by an assumed AOD from ~~pre-existing~~non-sulfate aerosol from the eruption to reach the measured AOD. **e)** Aerosol gravitational settling velocity (V_s) and

252   fit (equivalent aerodynamic diameter 1.1 μm) and average altitudes (z; right scale) of the HT-22 aerosol and

253   water vapor at latitudes -14 to -6°. **f)** Normalized stratospheric AOD evolution during one year for one wildfire

254   event (Martinsson et al., 2022) and two volcanic eruptions.

255   **Table 1.** Recent volcanic eruptions with SO_2 emissions, global stratospheric optical depths (AOD) and literature
256   references.

Date	Eruption	Short name	SO_2 (Tg)	SO_2 references	Global AOD[a]	Depolarization Ratio references
2008-08-07	Kasatochi	Ka-08	2	Yang et al., 2010	0.0061	Hoffmann et al., 2010
2009-06-12	Sarychev	Sa-09	1.09	Sandvik et al., 2021	0.0075	O'Neill et al., 2012
2011-06-12	Nabro	Na-11	1.5	Clarisse et a., 2012	0.0048	Zhuang & Yi 2016
2014-02-14	Kelut	Ke-14	0.18	Li et al., 2017	0.0014	Vernier et al., 2016
2015-04-23	Calbuco	Ca-15	0.3	Pardini et al., 2018	0.0035	Klekociuk et al., 2020
2019-06-22	Raikoke		1.5			
2019-06-26	Ulawun	RU-19	0.14	Kloss et al., 2021	0.0095	Voudouri et al., 2023
2019-08-03	Ulawun		0.3			
2021-04-10	Soufriere	So-21	0.31	Taylor et al., 2023	0.0016	[b]Lidar browse images
2022-01-15	Hunga Tonga	HT-22	0.45	Carn et al., 2022	0.0087	This work

257   [a] Global stratospheric AOD maximum increase due to the eruptions. References: Friberg et al., 2018 and this

258   work (2019 – 2023)

259   [b] Lidar Level 1 Browse Images - 2021-04-26 09:42:19Z - Section 1 (https://www-

260   calipso.larc.nasa.gov/products/lidar/browse_images/std_v451_index.php)

261   We adopt the central estimate of Carn et al. (2022), i.e., 0.45 Tg SO_2 with an e-folding time of ~6 days. The e-

262   folding time is unusually short for stratospheric conditions, probably due to elevated water vapor concentrations

263   (Carn et al., 2022). Fig. 5d shows the AOD, with double-sided 99.9% confidence interval of the mean in the

264   deep BD branch, where all the aerosol from the HT-22 eruption was injected (Fig. 4a). Using the AOD-to-SO_2

265   ratio based on six volcanic eruptions (Fig. 5c) to estimate the AOD based on the SO_2 emissions, we end up with

266   far too low AOD (Fig. 5d, broken line). To investigate the timing, we added 1.1 Tg excess SO_2 to reach the

267   measured AOD while preserving the measured e-folding time (dotted line). The excess SO_2 reaches into the

268   99.9% confidence interval of the average AOD after approximately 50% longer time from the eruption

269   compared to the time required for CALIOP to record a stable AOD. It is thus unlikely that the aerosol from the

270   HT-22 eruption was formed from SO_2 conversion alone, mainly because of the low SO_2 emissions, but also

271   because of the timing. Other material must have been present already the first days after the eruption. Making

272   use of the AOD-to-SO_2 ratio from Fig. 5c, adding ~~pre-existing~~non-sulfate aerosol from the HT-22 eruption

273   adjusted to obtain the measured AOD and using the measured SO_2 mass and e-folding time, results in the cyan

274   full line in Fig. 5d. Such a combination of ~~pre-existing~~non-sulfate aerosol from the eruption and SO_2 conversion

275   is consistent with the 99.9% confidence interval of the AOD average.

276   The next question is what is the source of the non-sulfate aerosol that ~~existing~~ was present before the conversion

277   of SO_2? We have no measurements of the aerosol composition to aid in this respect. From the depolarization

278   ratio (supplementary Fig. S2) we can rule out significant fractions of volcanic ash, which is also supported by

279   other measurements (Gupta et al., 2022; Carn et al., 2022). To find another plausible source of the ~~pre-~~

280   ~~existing~~non-sulfate aerosol we consider the intense sea – volcanism interaction during the HT-22 eruption

281   (Seabrook et al., 2023; Clare et al., 2023, Mastin et al., 2024, Millán et al., 2022) causing enhanced bubble

282   bursting (Keene et al., 2007) and/or explosive superheated water. Such events are not only sources of water

283   vapor but also releases the entire sea water substance to the atmosphere that includes sea salts. High

284   concentrations of sea salt in volcanic ash fallout from the HT-22 eruption has been documented (Colombier et

285   al., 2023). Sea salt particles enter the volcanic column together with the water vapor. As the particles are

286   hygroscopic, they readily serve as condensation nuclei in cloud formations as the air cools on the way up to the

287   stratosphere. In the competition for water, preferentially large particles are scavenged in cloud formations prior

288   to the formation of precipitation. This leaves the smaller particles as an interstitial aerosol (Martinsson et al.,

289   1999). The amount of aerosol from the eruption ~~existing~~ present before the SO_2 conversion (Fig. 5d) would

290   correspond to aerosol formation from 1.1 Tg SO_2 based on the AOD-to-SO_2 ratio (Fig. 5c). Using this number as

291   a coarse estimate we can compare it with the amount of water injected into the deep BD branch (137 Tg; Fig.

292   2b). With the typical salinity of sea water (35 g/kg) that amount of water corresponds to 4.8 Tg of sea salt,

293   which is four times the coarse estimate of ~~pre-existing~~non-sulfate aerosol mass.

294   Besides the water from enhanced bubble bursting induced by volcaniclastic density currents or explosive

295   superheated water, water evaporates directly from a heated ocean without sea salt emissions. Additional

296   quantitative uncertainties pertain to the relative losses of water and sea salt to precipitation. Given the orders of

297   magnitude of these estimates we can from this standpoint conclude that aerosol formation from strong sea –

298   volcanism interaction is a plausible source of a large fraction of the stratospheric aerosol from the HT-22

299   eruption. However, we also need to consider the low depolarization ratio of the HT-22 aerosol. Cubic sodium

300   chloride particles can according to modeling show depolarization ratios in the range 0 to approximately 0.25

301   with strong dependence on the particle size, being close to 0 for particle volume mean diameters less than 0.7 –

302   0.8 µm before it gradually increases (Murayama et al., 1999; Haarig et al., 2017). The ageing of sea salt particles

303   in the atmosphere tends to round the particles (Adachi and Buseck, 2015) thus reducing depolarizations. To

304   further investigate this matter, we need to consider the particle size distribution.

305   Several authors have reported on the stratospheric aerosol particle size following the HT-22 eruption, i.e., 0.6 –

306   1 µm diameter (Boichu et al.,2023), 0.8 µm (Duchamp et al., 2023) and 2 – 3 µm (Legras et al., 2022). Whereas

307   the former two estimates show good agreement, the latter, based on estimating the gravitational settling velocity,

308   stands out by finding the particles to be larger than the other estimates. We used the same method as Legras et

309   al., (2022) to estimate the settling velocity: V(sedimentation) = V(aerosol) – V(air), where V is the vertical

310   velocity, V(aerosol) the observed weekly change in the aerosol centroid altitude and V(air) is estimated from the

311   weekly change in the altitude of the water vapor centroid. Applying a 3-week moving average dampened

312   variations in settling velocity leading to Fig. 5e. The gravitational settling velocity varies around the value 20

313   m/day, agreeing well with the results of Legras et al. (2022) whereas the conversion to particle size differs. The

314   settling velocity of a given particle depends on the pressure and temperature because of the air viscosity and the

315   Cunningham slip correction factor's dependence on the mean free path of the air. We computed the particle size

316   that best fits the weekly settling velocity observations. Fig. 5e shows decreased settling velocity as the aerosol

317   falls to lower altitude. We found that the equivalent aerodynamic diameter was 1.1 µm, which is based on the

318   assumptions of a spherical particle shape and particle density of 1 g/cm^3. The low depolarization ratio

319   (supplementary Fig. S2) validates the first assumption. The density of the particles is not known a priori.

320   However, the low relative humidity (Figs. 5a and b) results in concentrated solution drops of sulfuric acid and

321   sea salts, having density clearly exceeding 1 g/cm^3, e.g., a 76.5% sulfuric acid – water solution has a density of

322 1.75 g/cm^3 at stratospheric conditions (Myhre et al., 1998). Applying that density results in 0.70 μm geometric

323 diameter and changing the density to 1.5 and 2 g/cm^3 results 0.81 and 0.62 μm diameter, respectively, which is

324 in good agreement with estimates based on other methods. Based on our results and others (Boichu et al., 2023;

325 Duchamp et al., 2023) we conclude that the HT-22 aerosol is submicron in diameter, in between stratospheric

326 background and Mt. Pinatubo particle sizes (Bauman et al., 2003; Wilson et al., 2008). The depolarization ratio

327 was low already the first days after the eruption when only a small fraction of the SO$_2$ conversion was

328 completed. However, the particle size of the HT-22 aerosol falls in the region where the depolarization ratio for

329 cubic sodium chloride particles is small, thus not contradicting that sea salt from volcanism – sea interaction

330 was a strong source of the HT-22 aerosol.

331 The water vapor injected into the deep BD branch remained in the stratosphere for the full two years of this

332 study, although 23% was transported from the deep BD branch to the shallow one 1.5 years after the eruption

333 (Fig. 2b). The stratospheric AOD remained almost constant for one year before starting to decline (Fig. 4a).

334 Because of gravitational settling aerosol remains in the stratosphere for a shorter time than gases with low

335 chemical reactivity. The combined effect of the 2019 Raikoke and Ulawun eruptions on the maximum global

336 stratospheric AOD is the highest observed for recent eruptions (Table 1) when also the lowest part of the

337 stratosphere are accounted for. The peak AOD from HT-22 eruption is slightly lower. However, the long

338 duration of the AOD from the HT-22 eruption, caused by the powerful eruption placing the effluents in the deep

339 BD branch in the tropics, makes it the most important in terms of stratospheric AOD since the 1991 eruption of

340 Mt. Pinatubo (Fig. 5f). The first year after the eruption the AOD was 0.016. Subtracting average background

341 AOD (Friberg et al., 2018) the stratospheric global mean AOD from the HT-22 eruption becomes 0.010. This

342 corresponds to -0.24 W/m^2 in global stratospheric total volcanic effective radiative forcing during the first year

343 after the eruption, according to results based on volcanic activity years 1979 to 2015 (Schmidt et al., 2018).

344 The HT-22 was the last major volcanic eruption to be studied based on data from the CALIOP lidar aboard the

345 CALIPSO satellite that ended its mission in June 2023. This is by far the most efficient method for studies of the

346 initial months of stratospheric aerosol formation following volcanic eruptions and wildfires, because of its

347 brilliant vertical resolution and optically short vertical path. Limb-viewing techniques suffer from event

348 termination (saturation) during 2 – 3 months after a major stratospheric aerosol event (Martinsson et al., 2022;

349 Fromm et al., 2014; Chen et al., 2018; DeLand, 2019). Fig. 5f illustrates the importance of CALIOP by showing

350 the AOD of two volcanic eruptions and one wildfire. Conversion of SO$_2$ formed the Raikoke aerosol, resulting

351 in 2 – 3 months delay before the AOD peaked which is the case for most volcanic eruptions (Friberg et al.,

352 2018). In contrast, sea salt aerosol from HT-22 ~~existing~~ present before the SO$_2$ conversion dominated its AOD

353 and we observed the maximum already after two weeks. That was the time required for the aerosol to become

354 dispersed enough to allow approximately ten CALIOP measurements per day in the volcanic effluents, thereby

355 reducing the uncertainty in the daily average. Another special case was the 2017 Canadian wildfire where we

356 observed a strong and rapid decline of the stratospheric AOD (Fig. 5f) indicative of photolytic loss of organic

357 aerosol (Martinsson et al., 2022). A study of the 2019/2020 Australian wildfire showed similar losses, where

358 also a complex feed of wildfire aerosol from the upper troposphere during 1 – 2 weeks after the fire was

359 identified (Friberg et al., 2023), thanks to the mentioned special properties of the CALIOP instrument. The

360 decommissioning of the ageing CALIOP in June 2023 severely diminishes future studies of aerosol formation
361 and losses in the stratosphere, prompting the need for new satellite-based lidar systems.

4 Conclusions

363 Aerosol and water vapor in the stratosphere emanating from the 15 January 2022 eruption in Hunga Tonga (HT-
364 22) is investigated using satellite-based instruments CALIOP and MLS. Most of its effluents were injected into
365 the deep branch of the stratospheric Brewer-Dobson (BD) circulation.

366 A small fraction of the record-breaking water vapor injections into the deep BD branch reached up to the
367 stratopause after 1.25 years in the stratosphere, whereas 23% was transported down to the shallow BD branch as
368 the water vapor spread vertically. The water vapor injected into the deep BD branch remained in the stratosphere
369 for the full two years of this study. The water vapor from the HT-22 eruption in the southern tropics steadily
370 increased its latitudinal coverage, first to the southern midlatitudes. After a year most of the global stratosphere
371 was covered with water vapor from the HT-22 eruption, before a reduction of the tropical stratospheric
372 concentration appeared as the BD circulation brought tropospheric air that was unaffected by the HT-22
373 eruption.

374 The aerosol and its precursor gases were initially at the same altitude as the water vapor from the HT-22
375 eruption, but gravitational settling of the aerosol particles gradually opened a gap in altitude which resulted in
376 the aerosol from the HT-22 eruption mainly appearing in the tropics and the southern hemisphere. The
377 stratospheric aerosol optical depth (AOD) remained constant for a year after the eruption, before transport out of
378 the stratosphere started. At the time of the decommission of the CALIOP instrument in June 2023, 50% of the
379 aerosol from the HT-22 eruption had been removed from the stratosphere.

380 The AOD level of the stratosphere was established already 2 weeks after the eruption and was unexpectedly
381 high for a modest injection of $0.4 - 0.5$ Tg SO_2. Given the exceptional water vapor amounts from the HT-22
382 eruption, we investigated if hygroscopic growth affected the aerosol optical properties. Despite the record-
383 breaking water vapor emissions, the average relative humidity remained below 5% in the dry stratosphere,
384 causing no or limited hygroscopic growth.

385 The gravitational settling velocity of the aerosol is estimated from the altitude evolution to ~20 m/day,
386 corresponding to an equivalent aerodynamic diameter of 1.1 μm at the altitude of the aerosol layer. Assuming
387 density of concentrated solution drops of $1.5 - 2$ g/cm^3 the geometrical diameter becomes $0.6 - 0.8$ μm.

388 Comparing eight recent volcanic eruptions we find that the global AOD per mass of SO_2 emitted from the HT-22
389 eruption is 4 times that of most other eruptions. The amount of SO_2 and ash emitted to the stratosphere was
390 unusually small for an eruption with volcanic explosivity index (VEI) of 6. Aerosol formation from intense
391 volcano – sea interaction provides sea salt aerosol as a plausible explanation for the unexpectedly high AOD.

392 The maximum global stratospheric AOD following the HT-22 eruption is among the highest observed in more
393 than 30 years. The injection in the deep branch of DB circulation prolonged the perturbation of the stratospheric

aerosol, making the HT-22 eruption the largest aerosol event since that of Mt. Pinatubo in 1991. The 1-year average global AOD of 0.01 from the HT-22 eruption can be estimated to -0.24 W/m^2 in global stratospheric total volcanic effective radiative forcing.

References

Adachi K. and P.R. Buseck, Changes in shape and composition of sea-salt particles upon aging in an urban atmosphere. Atmos. Environ. 100, 1-9, http://dx.doi.org/10.1016/j.atmosenv.2014.10.036, 2015.

Andersson, S. M., Martinsson, B. G., Friberg, J., Brenninkmeijer, C. A. M., Rauthe-Schöch, A., Hermann, M., van Velthoven, P. F. J., and Zahn, A.: Composition and evolution of volcanic aerosol from eruptions of Kasatochi, Sarychev and Eyjafjallajökull in 2008–2010 based on CARIBIC observations, Atmos. Chem. Phys., 13, 1781–1796, https://doi.org/10.5194/acp13-1781-2013, 2013.

Andersson, S. M., Martinsson, B. G., Vernier, J. P., Friberg, J., Brenninkmeijer, C. A. M., Hermann, M., van Velthoven, P. F. J., and Zahn, A.: Significant radiative impact of volcanic aerosol in the lowermost stratosphere, Nat. Commun., 6, 1–8, https://doi.org/10.1038/ncomms8692, 2015.

Bauman J. J., P. B. Russell, M. A. Geller, and P. Hamill, A stratospheric aerosol climatology from SAGE II and CLAES measurements: 2. Results and comparisons, 1984–1999, J. Geophys. Res., 108(D13), 4383, doi:10.1029/2002JD002993, 2003.

Bernath P., C. Boone, A. Pastorek, D. Cameron and M. Lecours, Satellite characterization of global stratospheric sulfate aerosols released by Tonga volcano. J. Quant. Spectrosc. Rad. Transf. 299, 108520, 2023.

Boichu M., R. Grandin, L. Blarel, B. Torres, Y. Derimian, P. Goloub, C. Brogniez, I. Chiapello, O. Dubovic, T. Mathurin, N. Pascal, M. Patou and J. Riedi, Growth and Global Persistence of Stratospheric Sulfate Aerosols From the 2022 Hunga Tonga–Hunga Ha'apai Volcanic Eruption. J. Geophys. Res. Atmos. 128, e2023JD039010. https://doi. org/10.1029/2023JD039010, 2023.

Bourassa, A. E., Zawada, D. J., Rieger, L. A., Warnock, T. W., Toohey, M., & Degenstein, D. A., Tomographic retrievals of Hunga Tonga-Hunga Ha'apai volcanic aerosol. Geophysical Research Letters, 50, e2022GL101978. https://doi. org/10.1029/2022GL101978, 2023.

Carn S.A., N.A. Krotkov, B.L. Fisher and C. Li, Out of the blue: Volcanic SO2 emissions during the 2021– 2022 eruptions of Hunga Tonga—Hunga Ha'apai (Tonga). Front. Earth Sci. 10:976962. doi: 10.3389/feart.2022.976962, 2022.

Carr J.L., A. Horváth, D.L. Wu, and M.D. Friberg, Stereo plume height and motion retrievals for the record-setting Hunga TongaHunga Ha'apai eruption of 15 January 2022. Geophysical Research Letters 49, e2022GL098131, https://doi.org/10.1029/2022GL098131, 2022.

Chen, Z., Bhartia, P. K., Loughman, R., Colarco, P., and De Land, M.: Improvement of stratospheric aerosol extinction re trieval from OMPS/LP using a new aerosol model, Atmos. Meas. Tech., 11, 6495– 6509, https://doi.org/10.5194/amt-11 6495-2018, 2018.

Clare M.A., I.A. Yeo, S. Watson, R. Wysoczanski, S. Seabrook, K. Mackay, J.E. Hunt, E. Lane, P.J. Talling, E. Pope, S. Cronin, M. Ribó, T. Kula, D. Tappin, S. Henrys, C. de Ronde, M. Urlaub, S. Kutterolf, S.

Fonua, S. Panuve, D. Veverka, R. Rapp, V. Kamalov and M. Williams, Fast and destructive density currents created by ocean-entering volcanic eruptions. Science 381, 1085–1092, 2023.

Clarisse L., D. Hurtmans, C. Clerbaux, J. Hadji-Lazaro, Y. Ngadi, and P.-F. Coheur, Retrieval of sulphur dioxide from the infrared atmospheric sounding interferometer (IASI). Atmos. Meas. Tech., 5, 581–594, 2012.

Colombier M., I. A. Ukstins, S. Tegtmeier, B. Scheu, S. J. Cronin, S. Thivet, J. Paredes-Mariño, C. Cimarelli, K.-U. Hess, T. Kula, F.H. Latu'ila and D. B. Dingwell, Atmosphere injection of sea salts during large explosive submarine volcanic eruptions. Scientific Reports 13:14435, https://doi.org/10.1038/s41598-023-41639-8, 2023.

DeLand, M.: Readme document for the Soumi-NPP OPMS LP L2 AER675 Daily product, Goddard Earth Sciences Data and Information Services Center (GES DISC), http://disc.gsfc.nasa.gov (last access: October 2021), 2019.

Duchamp C., F. Wrana, B. Legras, P. Sellitto, R. Belhadji and C. von Savigny, Observation of the Aerosol Plume From the 2022 Hunga Tonga—Hunga Ha'apai Eruption With SAGE III/ISS. Geophys. Res. Lett. 50, e2023GL105076, https://doi.org/10.1029/2023GL105076, 2023.

Friberg J., Martinsson B. G., Andersson S. M., Brenninkmeijer C. A. M., Hermann M., Van Velthoven P. F. J., and Zahn A., Sources of increase in lowermost stratospheric sulphurous and carbonaceous aerosol background concentrations during 1999–2008 derived from CARIBIC flights, Tellus B, 66, 23428, https://doi.org/10.3402/tellusb.v66.23428, 2014.

Friberg, J., Martinsson, B. G., Andersson, S. M., and Sandvik, O. S.: Volcanic impact on the climate– the stratospheric aerosol load in the period 2006–2015, Atmos. Chem. Phys., 18, 11149–11169, https://doi.org/10.5194/acp-18-11149-2018, 2018.

Friberg J., B.G. Martinsson, and M.K. Sporre, Short- and long-term stratospheric impact of smoke from the 2019–2020 Australian wildfires. Atmos. Chem. Phys., 23, 12557–12570, 2023 https://doi.org/10.5194/acp-23-12557-2023, 2023.

Fromm M., Lindsey D. T., Servranckx, R., Yue G., Trickl T., Sica R., Doucet P., and Godin-Beekmann S., The untold story of pyrocumulonimbus, B. Am. Meteorol. Soc., 91, 1193–1209, 2010.

Fromm, M., Kablick III, G., Nedoluha, G., Carboni, E., Grainger, R., Campbell, J., and Lewis, L.: Correcting the record of volcanic stratospheric aerosol impact: Nabro and Sarychev Peak, J. Geophys. Res.-Atmos., 119, 1–22, https://doi.org/10.1002/2014JD021507, 2014.

Fueglistaler S., Dessler A. E., Dunkerton T. J., Folkins I., Fu Q., and Ote P. W., Tropical tropopause layer, Rev, Geophys., 47, RG1004, https://doi.org/10.1029/2008RG000267, 2009.

Garofalo, L. A., Levin, E. J. T., Campos, T., Kreidenweis, S. N., and Farmer, D. K.: Emission and evolution of submicron organic aerosol in smoke from wildfires in the western United States. ACS Space Chem., 3, 1237–1247, 2019.

Gupta A.K., R. Bennartz, K.E. Fauria and T. Mittal, Eruption chronology of the December 2021 to January 2022 Hunga Tonga-Hunga Ha'apai eruption sequence. Comm. Earth Environm. 3:314, https://doi.org/10.1038/s43247-022-00606-3, 2022.

Haarig M., A. Ansmann, J. Gasteiger, K. Kandler, D. Althausen, H. Baars, M. Radenz, and D.A. Farrell, Dry versus wet marine particle optical properties: RH dependence of depolarization ratio, backscatter,

and extinction from multiwavelength lidar measurements during SALTRACE. Atmos. Chem. Phys., 17, 14199–14217, https://doi.org/10.5194/acp-17-14199-2017, 2017.

Haarig, M., Ansmann, A., Baars, H., Jimenez, C., Veselovskii, I., Engelmann, R., and Althausen, D.: Depolarization and lidar ratios at 355, 532, and 1064nm and microphysi cal properties of aged tropospheric and stratospheric Cana dian wildfire smoke, Atmos. Chem. Phys., 18, 11847–11861, https://doi.org/10.5194/acp-18-11847-2018, 2018.

Hoffmann A., C. Ritter, M. Stock, M. Maturilli, S. Eckhardt, A. Herber, and R. Neuber, Lidar measurements of the Kasatochi aerosol plume in August and September 2008 in Ny-Ålesund, Spitsbergen. J. Geophys. Res., 115, D00L12, doi:10.1029/2009JD013039, 2010.

Hu, Q., Goloub, P., Veselovskii, I., Bravo-Aranda, J.-A., Popovici, I. E., Podvin, T., Haeffelin, M., Lopatin, A., Dubovik, O., Pietras, C., Huang, X., Torres, B., and Chen, C.: Long-range transported Canadian smoke plumes in the lower stratosphere over northern France, Atmos. Chem. Phys., 19, 1173–1193, https://doi.org/10.5194/acp-19-1173-2019, 2019.

Kahn, R. A., Limbacher, J. A., Junghenn Noyes, K. T., Flower, V. J. B., Zamora, L. M., & McKee, K. F., Evolving particles in the 2022 Hunga Tonga— Hunga Ha'apai volcano eruption plume. J. Geophys. Res., 129, e2023JD039963. https://doi.org/10.1029/2023JD039963, 2024.

Keene W.C., H. Maring, J.R. Maben, D.J. Kieber, A.A.P. Pszenny, E.E. Dahl, M.A. Izaguirre, A.J. Davis, M.S. Long, X. Zhou, L. Smoydzin, and R. Sander, Chemical and physical characteristics of nascent aerosols produced by bursting bubbles at a model air-sea interface, J. Geophys. Res., 112, D21202, doi:10.1029/2007JD008464, 2007.

Khaykin S., A. Podglajen, F. Ploeger, J.-U. Grooß, F. Tence, S. Bekki, K. Khlopenkov, K. Bedka, L. Rieger,, A. Baron, S. Godin-Beekmann, B. Legras, P. Sellitto, T. Sakai, J. Barnes, O. Uchino, I. Morino, T. Nagai, R. Wing, G. Baumgarten, M. Gerding, V. Duflot, G. Payen, J. Jumelet, R. Querel, B. Liley, A. Bourassa, B. Clouser, A. Feofilov, A. Hauchecorne and F. Ravetta, Global perturbation of stratospheric water and aerosol burden by Hunga eruption. Comm. Earth Environm., 3:316, https://doi.org/10.1038/s43247-022-00652-x|www.nature.com/commsenv, 2022.

Klekociuk A.R., D.J. Ottaway, A.D. MacKinnon, I.M. Reid, L.M. Twigger and S.P. Alexander, Australian Lidar Measurements of Aerosol Layers Associated with the 2015 Calbuco Eruption. Atmosphere 11, 124, 2020.

Kloss C., G. Berthet, P. Sellitto, F. Ploeger, G. Taha, M. Tidiga, M. Eremenko, A. Bossolasco, F. Jégou, J.-B. Renard, and B. Legras, Stratospheric aerosol layer perturbation caused by the 2019 Raikoke and Ulawun eruptions and their radiative forcing. Atmos. Chem. Phys., 21, 535–560, 2021.

Kremser, S., Thomason, L. W., von Hobe, M., Hermann, M., Desh ler, T., Timmreck, C., Toohey, M., Stenke, A., Schwarz, J. P., Weigel, R., Fueglistaler, S., Prata, F. J., Vernier, J. P., Schlager, H., Barnes, J. E., Antuña-Marrero, J. C., Fairlie, D., Palm, M., Mahieu, E., Notholt, J., Rex, M., Bingen, C., Vanhellemont, F., Bourassa, A., Plane, J. M. C., Klocke, D., Carn, S. A., Clarisse, L., Trickl, T., Neely, R., James, A. D., Rieger, L., Wilson, J. C., and Meland, B.: Stratospheric aerosol– Observations, processes, and impact on climate, Rev. Geophys., 54, 278–335, https://doi.org/10.1002/2015RG000511, 2016.

Lambert, A., Read, W., and Livesey, N.: MLS/Aura Level 2 Water Vapor (H2O) Mixing Ratio V005, Greenbelt, MD, USA, Goddard Earth Sciences Data and Information Services Center (GES DISC), https://doi.org/10.5067/Aura/MLS/DATA2508, 2020.

Legras B., C. Duchamp, P. Sellitto, A. Podglajen, E. Carboni, R. Siddans, J.-U. Grooß, S. Khaykin, and F. Ploeger, The evolution and dynamics of the Hunga Tonga–Hunga Ha'apai sulfate aerosol plume in the stratosphere. Atmos. Chem. Phys., 22, 14957–14970, 2022.

Li C., N.A. Krotkov, S. Carn, Y. Zhang, R.J.D. Spurr, and J. Joiner, New-generation NASA Aura Ozone Monitoring Instrument (OMI) volcanic SO2 dataset: algorithm description, initial results, and continuation with the Suomi-NPP Ozone Mapping and Profiler Suite (OMPS). Atmos. Meas. Tech., 10, 445–458, 2017.

Livesey, N. J., Read, W. G., Wagner, P. A., Froidevaux, L., Santee, M. L., Schwartz, M. J., Lambert, A., Manney, G. L., Valle, L. F. M., Pumphrey, H. C., Fuller, R. A., Jarnot, R. F., Knosp, B. W., and Lay, R.R.: EOS MLS Version 5.0x Level2 and 3 data quality and description document, Tech. rep., Jet Propulsion Laboratory D734 105336 Rev. A, https://mls.jpl.nasa.gov/publications, 2020.

Martinsson B.G., G. Frank, S.-I. Cederfelt, E. Swietlicki, O.H. Berg, J. Zhou, K.N. Bower, C. Bradbury, W. Birmili, F. Stratmann, M. Wendisch, A. Wiedensohler, B.A. Yuskiewicz, Droplet nucleation and growth in orographic clouds in relation to the aerosol population. Atmos. Res. 50, 289–315, 1999.

Martinsson, B. G., Brenninkmeijer, C. A. M., Cam, S. A., Hermann, M., Heue,K.P., vanVelthoven, P. F. J., and Zahn, A.: Influence of the 2008 Kasatochi volcanic eruption on sulfurous and carbona ceous aerosol constituents in the lower stratosphere, Geophys. Res. Lett., 36, 1–5, https://doi.org/10.1029/2009GL038735, 2009.

Martinsson, B. G., Friberg, J., Sandvik, O. S., Hermann, M., van Velthoven, P. F. J., and Zahn, A.: Formation and composition of the UTLS aerosol, Npj Climate and Atmospheric Science, 2, 1–6, https://doi.org/10.1038/s41612-019-0097-1, 2019.

Martinsson, B. G., Friberg, J., Sandvik, O. S., and Sporre, M. K.: Five-satellite-sensor study of the rapid decline of wildfire smoke in the stratosphere, Atmos. Chem. Phys., 22, 3967–3984, https://doi.org/10.5194/acp-22-3967-2022, 2022.

Mastin L.G., A.R. Van Eaton and S.J. Cronin, Did steam boost the height and growth rate of the giant Hunga eruption plume? Bull. Volcanology 86:64, https://doi.org/10.1007/s00445-024-01749-1, 2024.

Millán, L., Santee, M. L., Lambert, A., Livesey, N. J., Werner, F., Schwartz, M. J., Pumphrey H.C., Manney G.L., Wang Y., Su H., Read W.G. and Froidevaux H.C., The Hunga Tonga-Hunga Ha'apai Hydration of the Stratosphere. Geophysical Research Letters, 49, e2022GL099381. https://doi.org/10.1029/2022GL099381, 2022.

Murayama T., H. Okamoto, N. Kaneyasu, H. Kamataki, and K. Miura, Application of lidar depolarization measurement in the atmospheric boundary layer: Effects of dust and sea-salt particles. J. Geophys. Res. 104, 31781-31792, 1999.

Murphy, D. M. and Koop, T., Review of the vapour pressures of ice and supercooled water for atmospheric applications, Q. J. Roy. Meteor. Soc., 131, 1539–1565, https://doi.org/10.1256/qj.04.94, 2005.

549 Murphy D. M., Cziczo D. J., Hudson P. K., and Thomson D. S., Carbonaceous material in aerosol particles

550   in the lower stratosphere and tropopause region, J. Geophys. Res., 112, D04203,

551   https://doi.org/10.1029/2006JD007297, 2007.

552 Myhre C.E.L., C.J. Nielsen, and O.W. Saastad, Density and Surface Tension of Aqueous H_2SO_4 at Low

553   Temperature. J. Chem. Eng. Data 43, 617-622, 1998.

554 Nedoluha G.E., Gomez R.M., Boyd I., Neal H., Allen D.R. and Lambert A., The spread of the Hunga Tonga

555   H2O plume in the middle atmosphere over the first two years since eruption. J. Geophys. Res. Atmos.

556   129, e2024JD040907. https://doi.org/10. 1029/2024JD040907, 2024.

557 O'Neill N.T., C. Perro, A. Saha, G. Lesins, T. J. Duck, E. W. Eloranta, G. J. Nott, A. Hoffman, M. L.

558   Karumudi, C. Ritter, A. Bourassa, I. Abboud, S. A. Carn, and V. Savastiouk, Properties of Sarychev

559   sulphate aerosols over the Arctic, J. Geophys. Res., 117, D04203, doi:10.1029/2011JD016838, 2012.

560 Pardini F., M. Burton, F. Arzilli, G. La Spina, M. Polacci, SO2 emissions, plume heights and magmatic

561   processes inferred from satellite data: The 2015 Calbuco eruptions. J. Volcanol. Geotherm. Res. 361,

562   12–24, 2018.

563 Poli P. and N.M. Shapiro, Rapid characterization of large volcanic eruptions: measuring the impulse of the

564   Hunga Tonga Ha'apai explosion from teleseismic waves. Geophys. Res. Letters 49, e2022GL098123.

565   https://doi. org/10.1029/2022GL098123, 2022.

566 Proud S.R., A.T. Prata and S. Schmauss, The January 2022 eruption of Hunga Tonga-Hunga Ha'apai

567   volcano reached the mesosphere. Science 378, 554–557, 2022.

568 Sandvik O.S., J. Friberg, M.K. Sporre, and B.G. Martinsson, Methodology to obtain highly resolved SO2

569   vertical profiles for representation of volcanic emissions in climate models. Atmos. Meas. Tech., 14,

570   7153–7165, 2021.

571 Schmidt, A., Mills M. J., Ghan S., Gregory J. M., Allan R. P., Andrews T., Bardeen C.G., Conley A., Forster

572   P.M., Gettelman A., Portmann R.W., Solomon S. And Toon O.B., Volcanic radiative forcing from 1979

573   to 2015. J. Geophys. Res. Atmos. 123, 12,491–12,508. https://doi.org/10.1029/2018JD028776, 2018.

574 Schoeberl, M. R., Wang, Y., Ueyama, R., Taha, G., Jensen, E., and Yu, W., Analysis and impact of the

575   Hunga Tonga-Hunga Ha'apai stratospheric water vapor plume. Geophysical Research Letters, 49,

576   e2022GL100248. https://doi. org/10.1029/2022GL100248, 2022.

577 Seabrook S., K. Mackay, S.J. Watson, M.A. Clare, J.E. Hunt, I.A. Yeo, E.M. Lane, M.R. Clark, R.

578   Wysoczanski, A.A. Rowden, T. Kula, L.J. Hoffmann, E. Armstrong and M.J.M. Williams,

579   Volcaniclastic density currents explain widespread and diverse seafloor impacts of the 2022 Hunga

580   Volcano eruption. Nat. Commun., 14:7881, https://doi.org/10.1038/s41467-023-43607-2, 2023.

581 Sellitto P., A. Podglajen, R. Belhadj, M. Boichu, E. Carboni, J. Cuesta, C. Duchamp, C. Kloss, R. Siddans,

582   N. Bègue, L. Blarel, F. Jegou, S. Khaykin, J.-B. Renard and B. Legras, The unexpected radiative

583   impact of the Hunga Tonga eruption of 15th January 2022. Comm. Earth Environm. 3:288

584   |https://doi.org/10.1038/s43247-022-00618-z, 2022.

585 Sellitto P., R. Siddans, R. Belhadj, E. Carboni, B. Legras, A. Podglajen, C. Duchamp, and B. Kerridge,

586   Observing the SO2 and Sulfate Aerosol Plumes From the 2022 Hunga Eruption With the Infrared

587   Atmospheric Sounding Interferometer (IASI). Geophys. Res. Lett. 51, e2023GL105565.

588   https://doi.org/10.1029/ 2023GL105565, 2024.

Taha, G., OMPS-NPP L2 LP Aerosol Extinction Vertical Pro f ile swath daily 3slit V2, Greenbelt, MD, USA, Goddard Earth Sciences Data and Information Services Center (GES DISC), https://doi.org/10.5067/CX2B9NW6FI27, 2020.

Taha, G., Loughman, R., Colarco, P. R., Zhu, T., Thomason, L. W., and Jaross, G., Tracking the 2022 Hunga Tonga-Hunga Ha'apai aerosol cloud in the upper and middle stratosphere using space-based observations. Geophysical Research Letters, 49, e2022GL100091. https://doi.org/10.1029/2022GL100091, 2022.

Taylor I.A., R.G. Grainger, A.T. Prata, S.R. Proud, T.A. Mather, and D.M. Pyle, Asatellite chronology of plumes from the April 2021 eruption of La Soufrière, St Vincent. Atmos. Chem. Phys., 23, 15209–15234, 2023.

Vernier J.-P., Thomason L. W., Pommereau J. P., Bourassa A., Pelon J., Garnier A., Hauchecorne A., Blanot L., Trepte C., Degenstein D., and Vargas F., Major influence of tropical volcanic eruptions on the stratospheric aerosol layer during the last decade, Geophys. Res. Lett., 38, 1–8, https://doi.org/10.1029/2011GL047563, 2011.

Vernier J.-P., D. Farlie, T. Deshler, M. Natarajan, T. Knepp, K. Foster, F.G. Weingold, K.M. Bedka, L. Thomason and C. Trepte, In situ and space-based observations of the Kelud volcanic plume: The persistence of ash in the lower stratosphere. J. Geophys. Res. Atmos. 121, 11,104–11,118, doi:10.1002/ 2016JD025344, 2016.

Voudouri K.A., K. Michailidis, M.-E. Koukouli, S. Rémy, A. Inness, G. Taha, G. Peletidou, N. Siomos, D. Balis and M. Parrington, Investigating a Persistent Stratospheric Aerosol Layer Observed over Southern Europe during 2019. Remote Sens. 15, 5394. https://doi.org/10.3390/rs15225394, 2023.

Waters, J. W., Froidevaux, L., Harwood, R., Jarnot, R., Pickett, H., Read, W., Siegel, P., Cofield, R., Filipiak, M., Flower, D., Holden, J., Lau, G., Livesey, N., Manney, G., Pumphrey, H., Santee, M., Wu, D., Cuddy, D., Lay, R., Loo, M., Perun, V., Schwartz, M., Stek, P., Thurstans, R., Boyles, M., Chandra, S., Chavez, M., Chen, G.-S., Chudasama, B., Dodge, R., Fuller, R., Girard, M., Jiang, J., Jiang, Y., Knosp, B., LaBelle, R., Lam, J., Lee, K., Miller, D., Oswald, J., Patel, N., Pukala, D., Quin tero, O., Scaff, D., Snyder, W., Tope, M., Wagner, P., and Walch, M.: The earth observing system microwave limb sounder (EOS MLS) on the Aura satellite, IEEE T. Geosci. Remote, 44, 1106 1121, 2006

Wilson J.C., S.-H. Lee, J. M. Reeves, C. A. Brock, H. H. Jonsson, B. G. Lafleur, M. Loewenstein, J. Podolske, E. Atlas, K. Boering, G. Toon, D. Fahey, T. P. Bui, G. Diskin, and F. Moore, Steady-state aerosol distributions in the extra-tropical, lower stratosphere and the processes that maintain them. Atmos. Chem. Phys., 8, 6617–6626, 2008.

Winker, D. M., Hunt, W. H., and McGill, M. J.: Initial performance assessment of CALIOP, Geophys. Res. Lett., 34, 1–5, https://doi.org/10.1029/2007GL030135, 2007.

Winker, D. M., Pelon, J., Coakley, J. A., Ackerman, S. A., Charl son, R. J., Colarco, P. R., Flamant, P., Fu, Q., Hoff, R. M., Kittaka, C., Kubar, T. L., Le Treut, H., McCormick, M. P., Mégie, G., Poole, L., Powell, K., Trepte, K., Vaughan, M. A., and Wielicki, B. A.: The CALIPSO mission– A global 3D view of aerosols and clouds, B. Am. Meteorol. Soc., 91, 1211–1229, https://doi.org/10.1175/2010BAMS3009.1, 2010.

628   Winkler P., The growth of atmospheric aerosol particles as a function of the relative humidity – II Improved
629   concept of mixed nuclei. Aerosol Sci. 4, 373-387, 1973.

630   Xu J., D. Li D., Z. Bai, M. Tao and J. Bian, Large Amounts of Water Vapor Were Injected into the
631   Stratosphere by the Hunga Tonga–Hunga Ha'apai Volcano Eruption. Atmosphere 13, 912. https://
632   doi.org/10.3390/atmos13060912, 2022.

633   Yang, K., X. Liu, P. K. Bhartia, N. A. Krotkov, S. A. Carn, E. J. Hughes, A. J. Krueger, R. J. D. Spurr, and
634   S. G. Trahan, Direct retrieval of sulfur dioxide amount and altitude from spaceborne hyperspectral UV
635   measurements: Theory and application. J. Geophys. Res., 115, D00L09, doi:10.1029/2010JD013982,
636   2010.

637   Zhu Y., C.G. Bardeen, S. Tilmes, M.J. Mills, X. Wang, V. Lynn Harvey G. Taha, D. Kinnison, R.W.
638   Portmann, P. Yu, K.H. Rosenlof, M. Avery, C. Kloss, C. Li,10, A.S. Glanville, L. Millán, T. Deshler, N.
639   Krotkov and O.B. Toon, Perturbations in stratospheric aerosol evolution due to the water-rich plume of
640   the 2022 Hunga-Tonga eruption. Comm. Earth Environm. 3:248, https://doi.org/10.1038/s43247-022-
641   00580-w, 2022.

642   Zhuang J. and F. Yi, Nabro aerosol evolution observed jointly by lidars at a mid-latitude site and CALIPSO.
643   Atmos. Environm. 140, 106-116, 2016.

644   *Data availability.* The data used are publicly available: CALIOP V4.51 lidar data (https://search.
645   earthdata.nasa.gov/search?fp=CALIPSO), and MLS data (version 5.0-1.0a, level 2) from https://disc.gsfc.nasa.
646   gov/datasets?page=1&keywords=ML2H2O_005.

647   *Author contributions.* BGM planned the study, undertook most of the data analysis and wrote the paper. JF
648   undertook part of the data analysis and MKS contributed. JF and MKS undertook data extraction and handling
649   for the data analysis. All authors participated in discussions and commented on the manuscript.

650   *Disclaimer.* The contact author and the co-authors declare that they have no competing interests.

651   *Acknowledgements.* Aerosol products from the CALIOP sensor were produced by NASA Langley Research
652   Center. Water vapor and temperature profiles from MLS are supplied by Goddard Earth Sciences Data and
653   Information Services Center.

654   *Financial support.* The Swedish National Space Agency, contract 2022-00157, Johan Friberg. The Crafoord
655   Foundation, contract 20240901, Johan Friberg. Formas, contract 2020-00997, Moa Sporre. The Swedish
656   Research Council 2022-02836, Moa Sporre.